

Fluctuations of lamellar structure prior to a lamellar→gyroid transition in a nonionic surfactant system

Masayuki Imai,¹ Ayako Kawaguchi,¹ Akira Saeki,² Kaori Nakaya,¹ Tadashi Kato,³ Kazuki Ito,⁴ and Yoshiyuki Amemiya⁵

¹*Faculty of Science, Ochanomizu University, Bunkyo, Tokyo 112-0012, Japan*

²*Department of Physics, Keio University, Yokohama 223-8522, Japan*

³*Graduate School of Science, Tokyo Metropolitan University, Hachioji, Tokyo 192-0397, Japan*

⁴*Institute of Applied Biochemistry, University of Tsukuba, Tsukuba, Ibaraki 305-8572, Japan*

⁵*Faculty of Engineering, The University of Tokyo, Bunkyo, Tokyo 113-8656, Japan*

(Received 9 August 1999; revised manuscript received 10 July 2000)

Fluctuations of lamellar structure prior to a lamellar→gyroid transition in a nonionic surfactant–water system has been investigated by means of small-angle x-ray scattering (SAXS) and differential scanning calorimeter measurements. For large ΔT ($\Delta T = T - T_{LG}$, where T is the temperature and T_{LG} the lamellar→gyroid transition temperature) in the lamellar phase, the SAXS profiles can be described by a Caillé correlation function for undulating lamellar structure. Approaching the temperature to the T_{LG} , an excess diffuse scattering grows at the lower Q (Q is the magnitude of scattering vector) side of the first lamellar peak. Highly oriented lamellar samples revealed that the excess diffuse scattering arises from in-plane density fluctuations. We attribute this diffuse scattering to the perforation fluctuation layer (PFL) structure and we show that the PFL is an equilibrium structure. At T_{LG} , the PFL transformed to the gyroid phase through a transient ordered structure having a rhombohedral symmetry.

PACS number(s): 64.70.Md, 47.20.Hw, 82.65.Dp, 68.10.-m

I. INTRODUCTION

One of the most fascinating properties of surfactant-water systems and block copolymers is their ability to form a variety of ordered mesophases, such as hexagonally ordered cylinders (C), lamellae (L), and a gyroid (G) structure having a bicontinuous cubic network with I_{a3d} symmetry. The similarity of the morphology and phase behaviors for surfactant-water systems and block copolymers suggests a universal nature of ordered mesophases originated from their incompatibility effects. Hence the behaviors of ordered mesophases have been the subject of the extensive experimental [1–9] and theoretical [10–15] investigations.

An important target of the order-order transition (OOT) studies is to reveal the kinetic pathways between the ordered mesophases. First, Raçon and Charvolin [1] found unique epitaxial relationships between the characteristic planes of the ordered phases in a $C_{12}E_6(CH_3(CH_2)_{11}(OCH_2CH_2)_6OH)$ -water system. The morphology transitions take place keeping the fixed orientation of each geometry, indicating unique pathways between the complicated ordered mesophases. Clerc *et al.* [2] investigated the kinetics of the $C \rightarrow G$ and $L \rightarrow G$ transitions in a nonionic surfactant system using a time-resolved x-ray diffraction technique and found that the transitions proceeded in a manner of a nucleation and growth mechanism having time constants of about 100 ms. Recently, identical epitaxial relationships and the nucleation and growth mechanism in the OOTs have been established in block copolymer systems [3–6].

Referring to the above experimental results, theoretical approaches to reveal the kinetics of the OOTs have been attempted extensively. Laradji *et al.* [10,11] have investigated the stability of the ordered mesophase in diblock copolymers and showed the most unstable fluctuation modes

leading to the OOTs (spinodal decomposition kinetics) using a theory of anisotropic composition fluctuations. Qi and Wang [12] have shown similar results using a time-dependent Ginzburg-Landau (TDGL) technique. A feature of these theoretical approaches is that the characteristic fluctuation modes bring the destination ordered mesophase. Such a characteristic fluctuation mode was observed experimentally in an OOT between the C phase and the body-centered-cubic spheres phase of a triblock copolymer system [9]. However, there is room for further study on this scenario [13]. In many experiments the OOTs proceed by the nucleation and growth manner, which does not agree with the spontaneous process. Matsen [14] demonstrated the nucleation and growth manner of the $C \leftrightarrow G$ transition using a self-consistent mean-field theory (SCFT). Moreover, Hajduk *et al.* [4] observed complex structure in the $L \rightarrow G$ transition, i.e., hexagonally perforated layer (HPL) morphology. They showed that this structure is a long-lived nonequilibrium state, which converts to the G morphology upon isothermal annealing. Then it is quite meaningful to elucidate the stability of the fluctuations around the equilibrium ordered mesophases prior to the OOTs.

The qualitative discussions developed in the block copolymer systems may be relevant to the surfactant systems exhibiting the same morphology phase diagrams, because presumably the topology of their free-energy surface is analogous [10]. Actually, Larson [15] showed that the morphology phase diagrams for the surfactant-water system are identical to those for the block copolymer system using Monte Carlo simulations. From an experimental point of view, surfactant solutions have several advantages to investigate the kinetics of the morphology transitions. (1) These morphologies can be easily controlled by changing temperature and concentration. (2) Perfectivity of the ordered mesophases gives sharp diffraction peaks, which make it pos-

sible to analyze fluctuations of the ordered meso phases in detail. (3) Interactions in the lamellar structure have been well investigated over the past two decades [16–20].

The purpose of this paper is to reveal fluctuations of the L phase prior to the $L \rightarrow G$ transition in the surfactant-water system using a small-angle x-ray diffraction (SAXS) technique with a synchrotron-radiation source and newly developed large area charged-coupled-device (CCD) detector [21,22]. The CCD detector has high spatial resolution, wide dynamic range, and high sensitivity. These features enable us to record the evolution of scattering functions during the morphology transitions under *in situ* conditions.

II. EXPERIMENT

We examined the $L \rightarrow G$ transition of a $C_{16}E_7(CH_3(CH_2)_{15}(OCH_2CH_2)OH-D_2O$ system [23]. The nonionic surfactant $C_{16}E_7$ was purchased from Nikko Chemicals, Inc., and used without further purification and deuterium oxide purchased from ISOTEC, Inc. (99.9%) was used after being degassed by bubbling of nitrogen to avoid oxidation of the ethylene oxide group of surfactants. The sample containing 55 wt % of $C_{16}E_7$ was sealed in a glass vial. For homogenization we annealed the sample for 3 h at about 55 °C and then held it at room temperature for 21 h. This annealing procedure was repeated about one week and then the samples were transferred to a temperature control cell with mica windows for simultaneous SAXS and differential scanning calorimeter (DSC) measurements developed by Yoshida [24], which regulate the temperature within ± 0.01 °C. Standard sample dimensions were a diameter of 3.0 mm and a thickness of 1.0 mm which brings the polycrystalline L phase. In order to obtain a highly oriented L phase, we used thin sample cells with a thickness of 50 μm [2]. The orientation of the L phase was checked by polarized optical microscope observations.

SAXS measurements were performed using a BL-15A instrument at the photon factory (PF) in the high-energy accelerator research organization (KEK) [21]. In this experiment we used a 1.5-Å wavelength x-ray beam having a $0.8 \times 0.8\text{-mm}^2$ square cross section. The scattered beam was recorded using the CCD area detector covering the scattering vector Q ($Q = 4\pi \sin \theta/\lambda$) range from 0.015 to 0.33 \AA^{-1} . The obtained scattering patterns were corrected for the nonuniformity, image distortion, and background scattering.

A SEIKO differential scanning calorimetry (DSC) apparatus DSC5200 with a thermal analysis system 5600 was used to examine the thermodynamical stability of the L phase. The samples with about 60-mg weight were sealed in silver DSC pans used for liquid samples. Samples were heated from room temperature (~ 30 °C) to 80 °C with various heating rates (0.1, 0.5, and 1.0 °C/min) and then cooled to room temperature with a cooling rate of 0.1 °C/min. The obtained DSC diagrams were calibrated using standard sapphire sample.

III. RESULTS AND DISCUSSION

We show brief features of the $L \rightarrow G$ transition of a $C_{16}E_7/D_2O$ system obtained from the polycrystalline samples. According to the phase diagram for the $C_{16}E_7/D_2O$

system in Ref. [23], the 55 wt % sample has the $C \rightarrow G$ and $G \rightarrow L$ transition temperature at 42 and 48 °C, respectively. (Here the term “ L phase” expresses the stacked layer structure. The structure of the “ L phase” close to the $L \rightarrow G$ transition temperature (T_{LG}) will be discussed later.) The sample was heated from 34 °C (C phase) to 67 °C (L phase) and then annealed isothermally (± 0.1 °C) for 100 min to reduce the sample history. After the isothermal annealing, the sample was cooled from 67 °C to the T_{LG} with a stepwise manner. At the predetermined temperatures we measured SAXS patterns at intervals of 10 min in order to check the equilibrium structure. After the scattering patterns reached to the equilibrium, we decreased the temperature to the next step temperature. Especially in the vicinity of the T_{LG} , we carefully decreased the temperature with intervals of 0.1 °C and waited 30 min to examine the existence of the incubation time. The DSC measurements showed the $G \rightarrow L$ transition temperature (T_{GL}) of 51.6 °C (heating rate: 0.1 °C/min) and the T_{LG} of 46.2 °C (cooling rate: 0.1 °C/min). The T_{LG} obtained from SAXS experiments is slightly different from the average value [$(T_{LG} + T_{GL})/2 = 48.6$ °C] of the $L \leftrightarrow G$ transition temperature obtained from the DSC measurements. Hereafter we employ 48.6 °C as the T_{LG} .

Figure 1 shows the evolution of the two-dimensional (2D) scattering patterns from the L phase to the G phase in the cooling process. In the L phase [Fig. 1(a)], the scattering pattern shows isotropic Debye rings, indicating a randomly oriented polycrystalline state. When the temperature is decreased to 48.3 °C, new diffraction spots appears both inside and outside the first lamellar ring after the incubation time of 15 min during which the scattering keeps the double-ring pattern [Fig. 1(b)]. Decreasing the temperature to 47.9 °C, numerous spots increase their intensities and simultaneously the lamellar rings decrease their intensities [Fig. 1(c)].

Surprisingly when we decreased the temperature to 44.6 °C, diffraction peaks at inside of the first lamellar peak disappears and alternative diffraction peaks appear as shown in Fig. 1(d). Here we make clear this complicated $L \rightarrow G$ transition behavior. In Fig. 2 we plot the development of one-dimensional scattering profiles obtained by a circular average of the 2D patterns as a function of temperature. In the L phase, two Bragg peaks can be seen. The first and second peak positions are $Q_0 = 0.098 \text{\AA}^{-1}$ and 0.19\AA^{-1} , respectively, indicating stacked lamellar structure. Decreasing the temperature to the T_{LG} , the peak positions shift to the higher Q side and a diffuse shoulder appears at $Q = 0.09 \text{\AA}^{-1}$. At 47.5 °C, in addition to the lamellar peaks the scattering profile shows apparent new peaks at $Q = 0.093$ and 0.107\AA^{-1} whose ratio is close to $\sqrt{3}/2$ [25]. We also observed new weak peaks at $Q = 0.15$, 0.16 , and 0.19\AA^{-1} . It should be noted that the scattering profile at 47.5 °C does not always represent an equilibrium structure.

When we decreased the temperature to 43.8 °C, the scattering profile changed to another pattern. In Table I we list the new diffraction peaks with indices of the G structure (I_{a3d}). The agreement between the predicted and observed peak positions indicates that the latter ordered phase is the G phase and the former structure is a transient structure between the L and G phases. Holmes and co-workers investigated phase behavior of C_iE_j/D_2O systems and reported intermediate phases between the C phase and L phase or the cubic phase and L phase [26]. They attributed the intermedi-

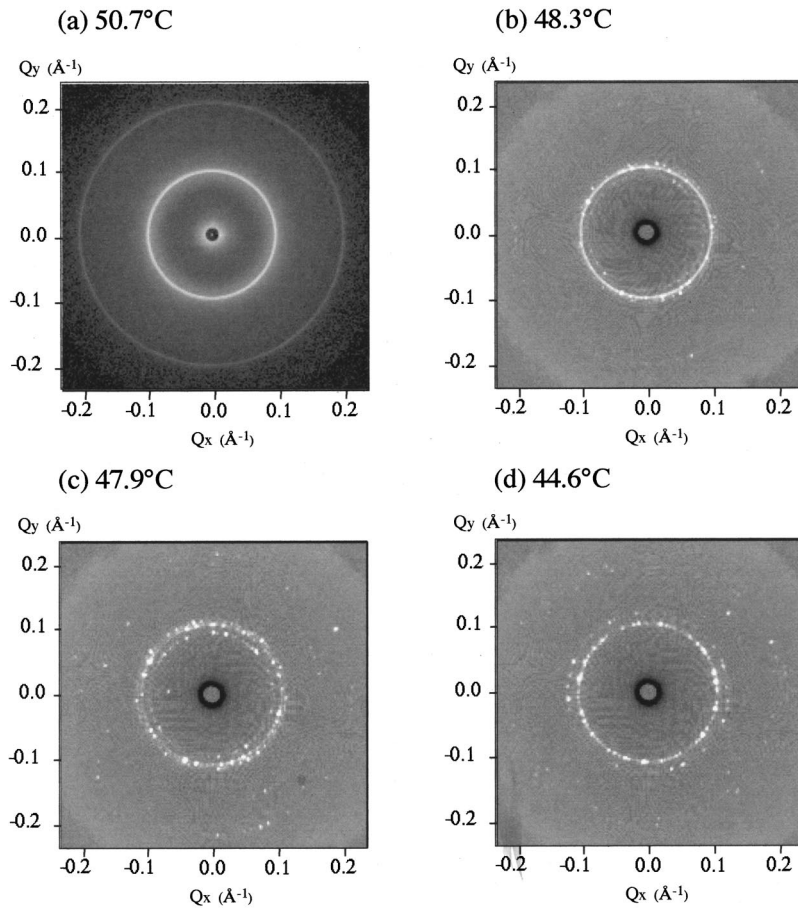


FIG. 1. Evolution of 2D small-angle x-ray scattering patterns from the L phase to the G phase. (a) 50.7 °C (lamellar phase), (b) 48.3 °C, (c) 47.9 °C, and (d) 44.6 °C.

ate phases to rhombohedral structures. The intermediate phase having space group of $R\bar{3}m$ provides the most likely structure which explains the diffraction pattern of the transient structure observed in this study (Table II). In this paper

we assign the transient structure to the rhombohedral (R) structure. In our experiment the R structure is only observed on cooling from the L phase to the G phase and not observed on heating from the G phase to the L phase. Furthermore, Fig. 3 shows the time evolution of the R structure at 47.9 °C. With the elapse of time, the polycrystalline R structure transforms to the G phase in a monodomain state spontaneously. Thus the R structure is not an equilibrium structure but a metastable structure and the $L \rightarrow G$ transition proceeds via the transient R structure. The kinetic pathway from the L phase to the G phase via the R structure will be discussed in a forthcoming paper and hereafter we focus our attention to fluctuations in the lamellar structure prior to the $L \rightarrow G$ transition.

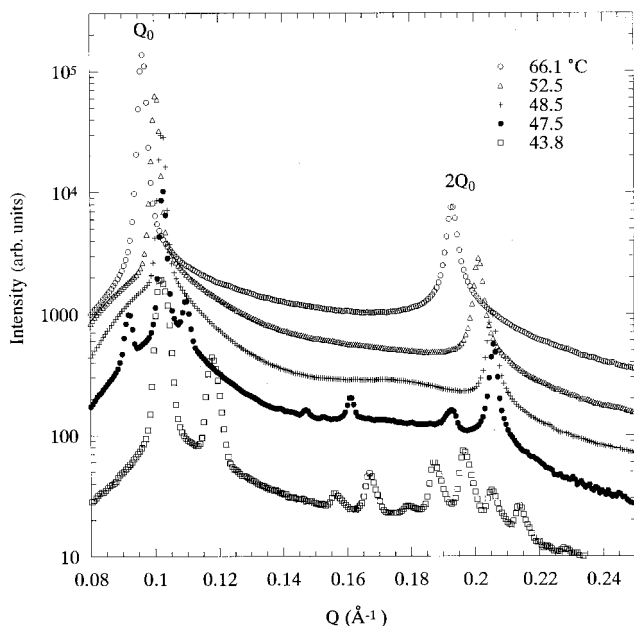


FIG. 2. Evolution of small-angle x-ray scattering profiles from the L phase to the G phase as a function of temperature. For convenience each profile is shifted along the intensity axis.

TABLE I. List of peak positions at 43.8 °C in Fig. 2 and indices based on the G phase with a unit-cell dimension of 150.3 Å.

Peak position (Å ⁻¹)	d spacing (Å)	Gyroid (Å) (hkl)	d_{cal} (Å)
0.102	61.36	(211)	61.3
0.118	53.25	(220)	53.1
0.156	40.28	(321)	40.2
0.167	37.58	(400)	37.6
0.179	35.14		
0.187	33.56	(420)	33.6
0.197	31.93	(332)	32.0
0.205	30.68	(422)	30.7
0.214	29.41	(431)	29.5

TABLE II. List of peak positions at 47.5 °C in Fig. 2 and indices based on the rhombohedral structure ($R\bar{3}m$) with unit-cell dimensions of $a=130.7 \text{ \AA}$ and $c=175.5 \text{ \AA}$ (vw means very weak peak intensity).

Peak position (\AA^{-1})	d spacing (\AA)	Rhombohedral model	
		(hkl)	d_{cal} (\AA)
0.0919	68.37	(110)	68.3
0.1098	57.22	(003)	58.5
vw		(103)	52.4
0.1474	42.63		
0.1612	38.98	(300)	39.4
0.1928	32.59	(310)	32.8
0.2058	30.53	(006)	29.3

Development of the scattering profile around the first lamellar peak from the L phase to the R structure is shown in Fig. 4. The scattering profile at 66.1 °C is composed of a sharp Bragg peak at $Q_0=0.098 \text{ \AA}^{-1}$ and a diffuse asymmetric tail spread around the Bragg peak. The diffuse tail originates from the undulation of lamellae [16–18] and can be described by the Caillé correlation function [19]. Caillé derived a correlation function for the undulating lamellae using bulk moduli for layer compression B and layer curvature K

$$S(R)=S(z,\rho)\sim(1/\rho)^2\eta\exp\{-\eta[2\gamma+E_1(\rho^2/4\lambda z)]\}, \quad (1)$$

$$\eta=Q_0^2kT/8\pi(BK)^{1/2}, \quad (2)$$

where $R^2=z^2+\rho^2$ with $\rho^2=x^2+y^2$, the z direction is normal to the layers, γ is Euler's constant, $E_1(x)$ is the exponential integral function, Q_0 is the first peak position, and $\lambda=(K/B)^{1/2}$. The powder-averaged scattering function obtained from the correlation function is given by

$$S(Q)\sim\int_{-\infty}^{\infty}dz\int_0^{\infty}d\rho S(z,\rho)e^{-R^2\pi/L^2}[(\sin QR)/QR]e^{-iGz}, \quad (3)$$

where L is the domain size and $G=mQ_0$ ($m=1,2,\dots$). For large $Q-Q_0\geq 2\pi/L$, the scattering profile exhibits power-law behavior $S(Q)\sim|Q-Q_0|^{-P}$ with $P=1-\eta$. The inset (66.1 °C) in Fig. 4 shows the fitting results at 66.1 °C based on Eq. (3) convoluted with a Gaussian resolution function with half-width at half-maximum of $2\times 10^{-4} \text{ \AA}^{-1}$. The parameter values obtained from this fitting are $\eta=0.3$ and $\lambda=5.0 \text{ \AA}$, which give the elastic constant B of $1.6\times 10^{20}k_B T$ and the bending modulus κ of $0.7k_B T$, where κ is derived from K through the relation $\kappa=Kd$ (d is the lamellar distance). The obtained κ value is close to the thermal energy, which agrees well with the results reported for the lyotropic lamellar phase of a microemulsion system [17]. Thus in this temperature region, the surfactant membrane has the undulation fluctuated lamellar structure.

Decreasing the temperature to the T_{LG} , additional diffuse scattering begins to grow at the lower Q side of the Bragg peak ($Q\sim 0.09 \text{ \AA}^{-1}$) (Fig. 4). This new diffuse shoulder cannot be explained by the Caillé correlation function, indicat

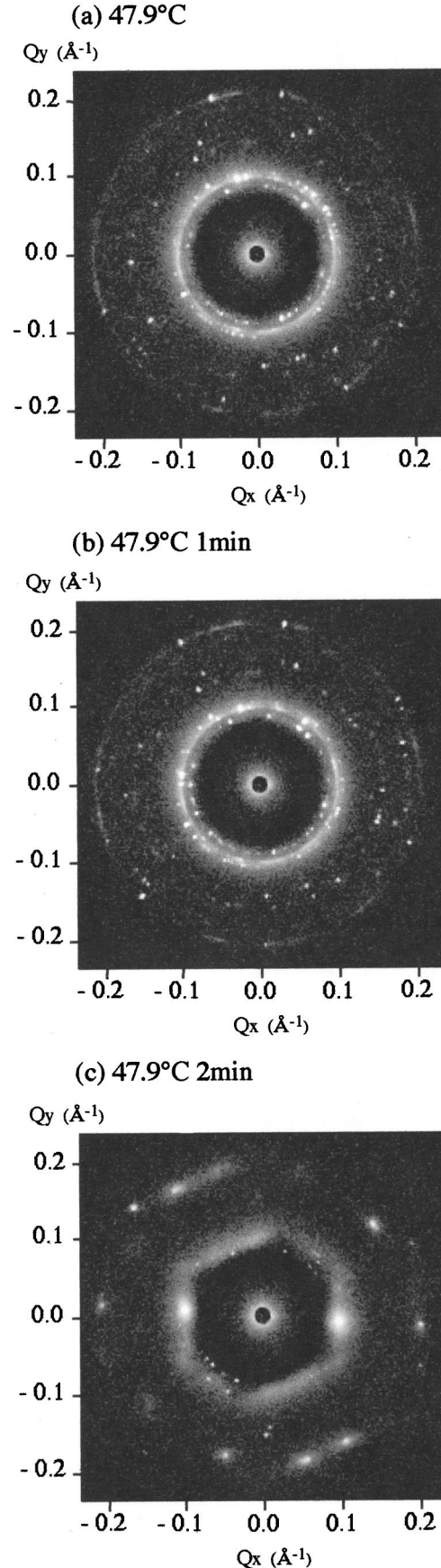


FIG. 3. Time evolution of 2D small-angle x-ray scattering profiles at 47.9 °C (from the R structure to the G phase).

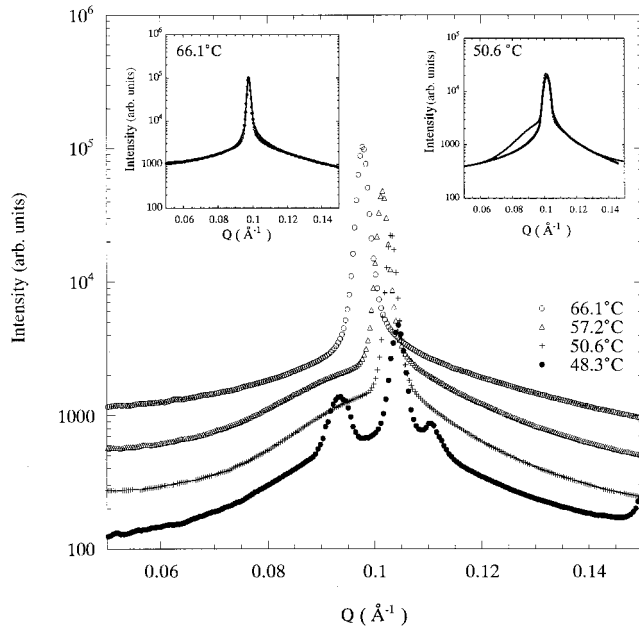


FIG. 4. Evolution of small-angle x-ray scattering profiles around the first lamellar peak from the L phase to the G phase as a function of temperature. For convenience each profile is shifted along the intensity axis. Inset figures show the result of the fitting of an experimental profile for 66.1 °C and 50.6 °C by the Caillé correlation function (solid line).

ing the existence of another type of fluctuations. The inset (50.6 °C) clearly demonstrates the excess diffuse scattering deviated from the Caillé function (solid line). In order to clarify the behavior of the diffuse shoulder, we subtracted the Caillé power-law component from the observed scattering profiles. The resultant diffuse profiles can be described by a function of the form $S_{sh}(Q) = a/[(Q - Q_d)^2 + \xi^{-2}]$, where a and ξ are constants and Q_d is the position giving maximum

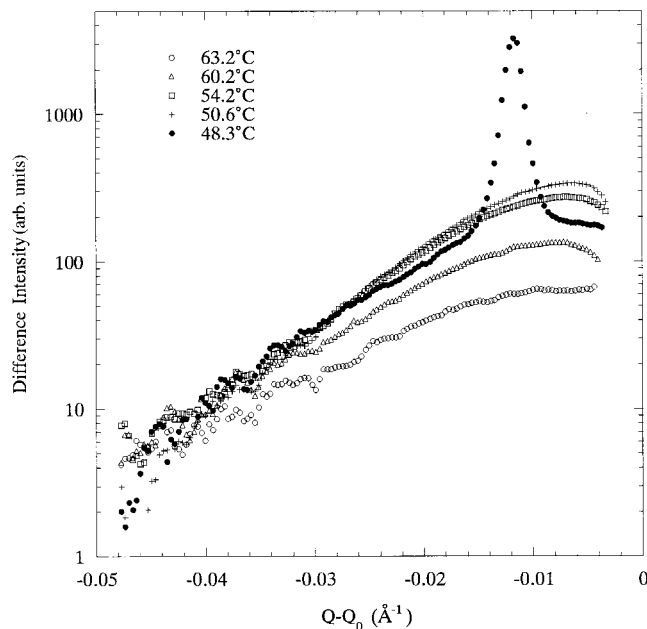
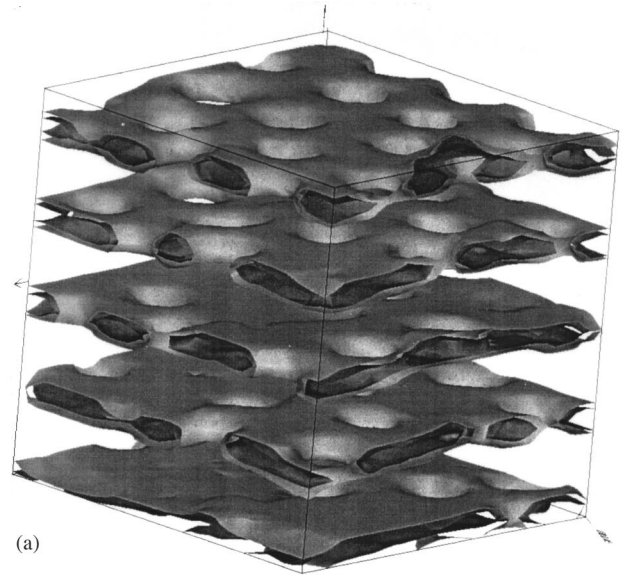
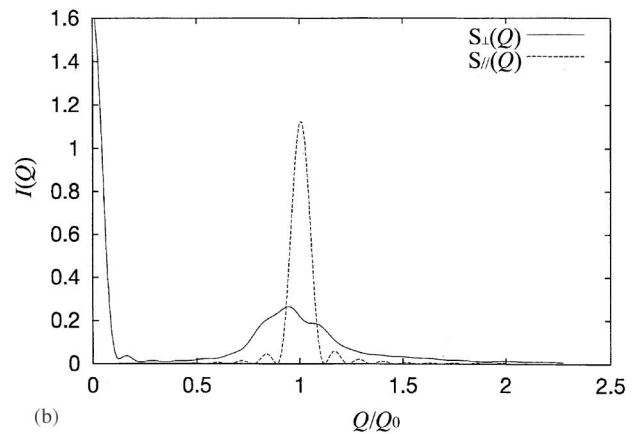


FIG. 5. Evolution of excess diffuse scattering profiles as a function of temperature. The horizontal axis is $Q - Q_0$, where Q_0 is the first peak position of the lamellar structure.



(a)



(b)

FIG. 6. (a) Perforating lamellar structure obtained in Saeki's simulation [28]. (b) Scattering functions of the PFL structure. $S_{\perp}(Q)$ is the perpendicular component to the lamellar plane and $S_{\parallel}(Q)$ is the parallel component to lamellar plane.

intensity of the diffuse scattering. Thus the excess scattering has a maximum at $Q_d (\neq Q_0)$.

In Fig. 5 we plot the subtracted diffuse shoulder scattering profiles against $Q - Q_0$ at different temperatures. Decreasing the temperature from $T = 63.2$ °C to the T_{LG} , the intensity of the excess diffuse scattering increases with keeping the peak maximum position. The diffuse scattering profiles were reversible against the temperature. At 48.3 °C, the diffuse shoulder transforms to the sharp peak attributed to the (110) spacing of the R structure. The agreement between the positions of the diffuse shoulder and the (110) peak of the R structure indicates that the transformation to the R structure proceeds using a characteristic length of the new fluctuation mode of lamellae.

Qi and Wang [27] investigated the stability of the L phase using a Leibler free-energy functional and found that the least stable fluctuations appear when the L phase closes to its spinodal. Recently Saeki and co-workers [28,29] developed a computational simulation scheme to obtain the equilibrium structure of ordered mesophases. They introduced a time derivative of the local order parameter ψ to the time-dependent Ginzburg-Landau scheme and constructed the following couple of kinetic equation:

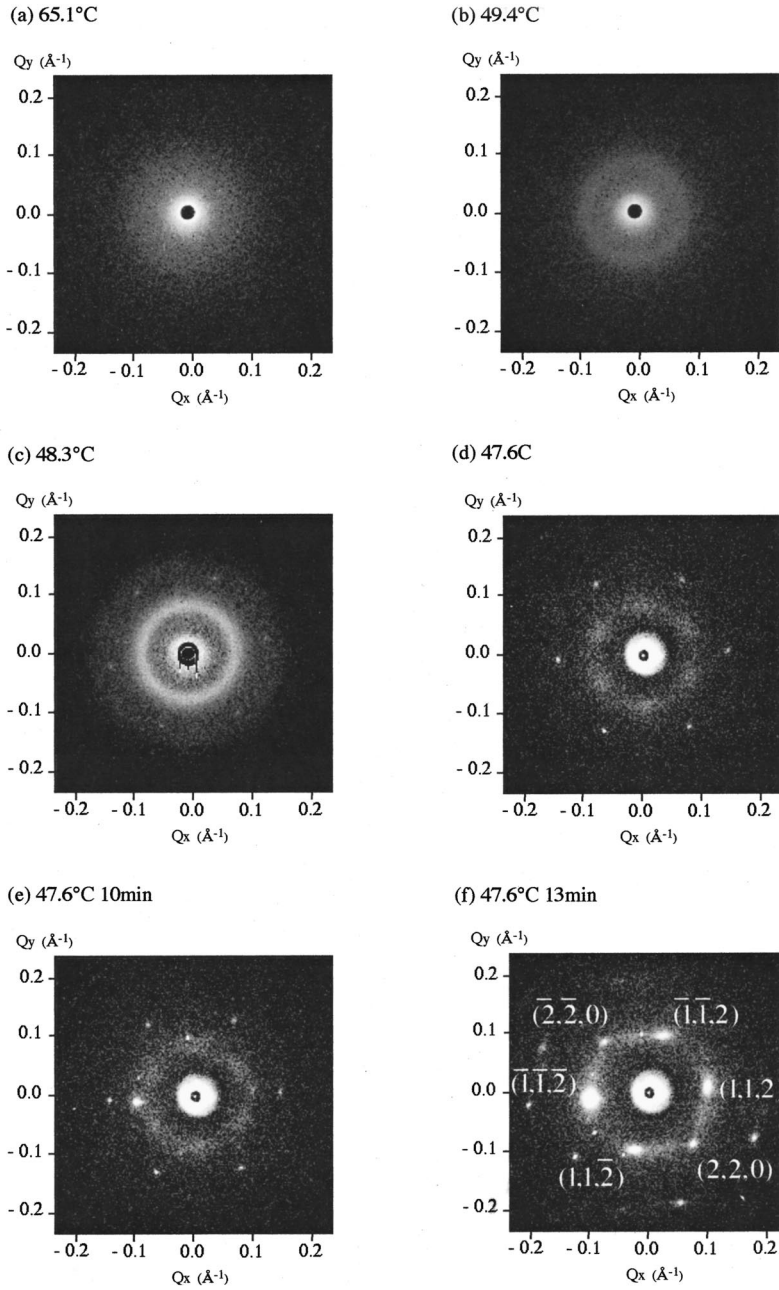


FIG. 7. Evolution of 2D scattering patterns $S_{\perp}(Q_x, Q_y)$ from the L phase to the G phase (a) 65.1 °C, (b) 49.4 °C, (c) 48.3 °C, and (d)–(f) time evolution of scattering patterns at 47.6 °C.

$$\frac{\partial}{\partial t} \phi(\mathbf{r}) = \Delta(-A\psi + u\psi^3 - D\Delta\psi) - B[\psi - 1 + 2f], \quad (4)$$

$$\frac{\partial}{\partial t} \psi(\mathbf{r}) = \phi(\mathbf{r}). \quad (5)$$

The velocity field $\phi(\mathbf{r})$ plays a role in accelerating the convergence of the kinetic equation to the equilibrium structure. Using this scheme, Saeki found perforated lamellae close to the T_{LG} as shown in Fig. 6(a). The channels in the lamellae fluctuate with time and do not show characteristic spatial symmetries such as hexagonal symmetry observed in block copolymers (HPL phase). Thus, this structure is not the HPL phase but the perforation fluctuation layer (PFL) structure. The corresponding scattering functions of the PFL for parallel $S_{\parallel}(Q)$ and perpendicular $S_{\perp}(Q)$ to the lamellar plane are shown in Fig. 6(b). A sharp Bragg peak in the $S_{\parallel}(Q)$ profile

corresponds to the lamellar spacing. It should be noted that a diffuse peak appears in $S_{\perp}(Q)$ at a slightly lower Q side of the first lamellar peak position. The existence of the diffuse peak indicates that the interchannel distance has a characteristic length although the PFL structure does not have long-range order. These results suggest that the experimentally observed diffuse peak originates from the PFL structure.

In order to confirm the validity of the PFL model we performed scattering experiments for oriented lamellae, which reveals the behavior of in-plane and out-of-plane fluctuations. Figure 7 shows the evolution of the 2D scattering patterns, $S_{\perp}(Q_x, Q_y)$, during the cooling process from the L phase to the G phase when the x-ray beam irradiates perpendicular to the lamellar plane. The scattering pattern at 65.1 °C [Fig. 7(a)] is monotonic without Bragg peaks confirming that the x-ray beam irradiates perpendicular to the lamellar plane. Decreasing the temperature to the T_{LG} , a

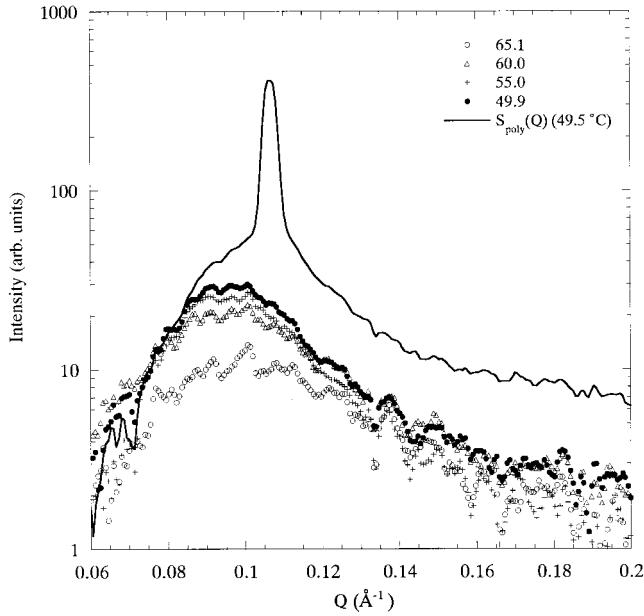


FIG. 8. Evolution of $S_{\perp}(Q)$ from the L phase to the G phase as a function of temperature with the scattering function of polycrystalline lamellar $S_{\text{poly}}(Q)$ 49.5 °C.

diffuse isotropic scattering ring appears [Fig. 7(b)], indicating the development of the in-plane density fluctuations. Figure 8 shows the temperature dependence of $S_{\perp}(Q)$ obtained by the circular average of the 2D scattering patterns with a scattering function of the polycrystalline lamellae, $S_{\text{poly}}(Q)$ at 49.5 °C. The in-plane density fluctuations give a diffuse peak at $Q_d \sim 0.09 \text{ \AA}^{-1}$ and the peak position is the slightly lower Q side of the first lamellar peak, which agrees well with the PFL model of the Saeki's simulation. Thus, channels in lamellae have the short-range order with an isotropic in-plane arrangement but the long-range order. Decreasing the temperature from 65.1 °C to the T_{LG} , the intensity of the diffuse peak increased as observed in the polycrystalline sample. The diffuse excess scattering observed in the polycrystalline sample arises from the PFL structure.

It should be remarked that the HPL (PL) structure frequently observed in block copolymers [4,5] may explain the observed SAXS pattern for the polycrystalline sample. However, this model can be excluded because of the diffuse scattering peak profile and the absence of higher-order reflections characteristic to the HPL (PL) structure in the scattering pattern for the oriented lamellae (see Figs. 7 and 8). Hajduk *et al.* showed that the characteristic feature of the scattering profile for PL is decreased in the intensity of the second-order lamellar peak compared to the first-order one [4,5]. Figure 2 clearly shows that the growth of the diffuse excess scattering does not accompany a decrease in the second-order lamellar reflection. Thus the PFL structure is the most appropriate to explain observed diffuse scattering.

When the temperature approaches the T_{LG} the intensity of the diffuse ring increases. At 47.6 °C hexagonal diffraction spots (corresponding to diffraction spots from $\{300\}$ crystal planes) of the R structure appear with hexagonally symmetry diffuse fragments [Figs. 7(c) and 7(d)]. With further annealing at 47.6 °C the scattering pattern transforms to the typical G phase pattern [Figs. 7(e) and 7(f)]. Here it should be noted that diffraction spots from $\{211\}$ crystal planes appear at the

diffuse peak position of the R structure. The kinetics of the $L \rightarrow G$ transition is fairly complicated and so we will discuss this matter in a future paper.

Before we discuss the nature of the PFL, we examine the behavior of the undulation fluctuations. If we irradiate x-ray beam parallel to the lamellar plane, we can estimate the undulation mode of the lamellar structure. Figure 9(a) shows the 2D scattering pattern under the parallel condition, $S_{\parallel}(Q_z, Q_x)$ at 63.0 °C. The scattering pattern has two intense spots on the ring, indicating a high orientation of the lamellae. Figure 9(b) shows the temperature dependence of the $S_{\parallel}(Q)$, obtained by sector averaging to the Q_z direction. The scattering function shows a sharp Bragg peak with a diffuse asymmetric tail spread around the Bragg peak, which is a typical profile for the undulating lamellae as described before. Decreasing the temperature to the T_{LG} , the diffuse tail keeps its profile and the excess diffuse scattering at the lower Q side of the Bragg peak does not grow. Thus the amplitude of undulation fluctuations does not change significantly prior to the $L \rightarrow G$ transition and so we can conclude that the PFL is responsible for the diffuse excess scattering observed for the polycrystalline sample.

As mentioned in the Introduction, Hajduk *et al.* [4,5] observed the HPL (PL) morphology prior to the $L \rightarrow G$ transition in block copolymers. They showed that these structures are long-lived nonequilibrium states, which convert to the gyroid morphology upon isothermal annealing. Thus the PL structure is metastable [13]. Then it is quite important to examine the thermodynamical stability of the PFL structure observed in the surfactant-water system. In the SAXS experiments, we confirmed the reversibility of the diffuse scattering function against temperature for polycrystalline and highly oriented samples, which suggests the PFL is equilibrium structure. Here we show results of DSC experiments. Heat flows of the sample for the heating process from room temperature (C phase) to 80 °C (L phase [23]) with a rate of 0.1 °C/min and for the cooling process from 80 °C to room temperature with a rate of 0.1 °C/min are shown in Fig. 10. For both heating and cooling processes, the $L \leftrightarrow G$ transition gives sharp peaks, although the transition has thermal hysteresis of about 5 °C. Here we cannot observe the latent heat of the $L \rightarrow R$ transition. This may be due to the very slow cooling rate. The latent heats of the $L \rightarrow G$ transition and $G \rightarrow L$ transition were 0.5 mJ/mg for both.

On the heating process after the $L \rightarrow G$ transition, the DSC curve shows a broad weak exothermic peak around 65 °C and a corresponding endothermic peak is observed on the cooling process as shown in Fig. 10. In the SAXS experiments, the intensity of the excess diffuse scattering begins to increase around 65 °C and becomes constant at 52 °C. The agreement between the behavior of the SAXS profiles and the latent heat peaks in the DSC measurements indicates that the latent heat is due to the formation of the PFL structure. Thus the PFL structure in the surfactant-water system is a thermodynamically equilibrium state. On the contrary, the HPL (PL) in block copolymers is a metastable state and transforms to the G phase spontaneously. According to the fitting of the SAXS profiles of this system based on the procedure of Nallet *et al.* [20], we obtained a hydrophobic bilayer thickness $\delta_c = 14.4 \pm 0.04 \text{ \AA}$, a hydrophilic layer thickness $\delta_h = 19.9 \pm 1.3 \text{ \AA}$ (bilayer thickness $\delta = 54.2 \pm 3.0 \text{ \AA}$),

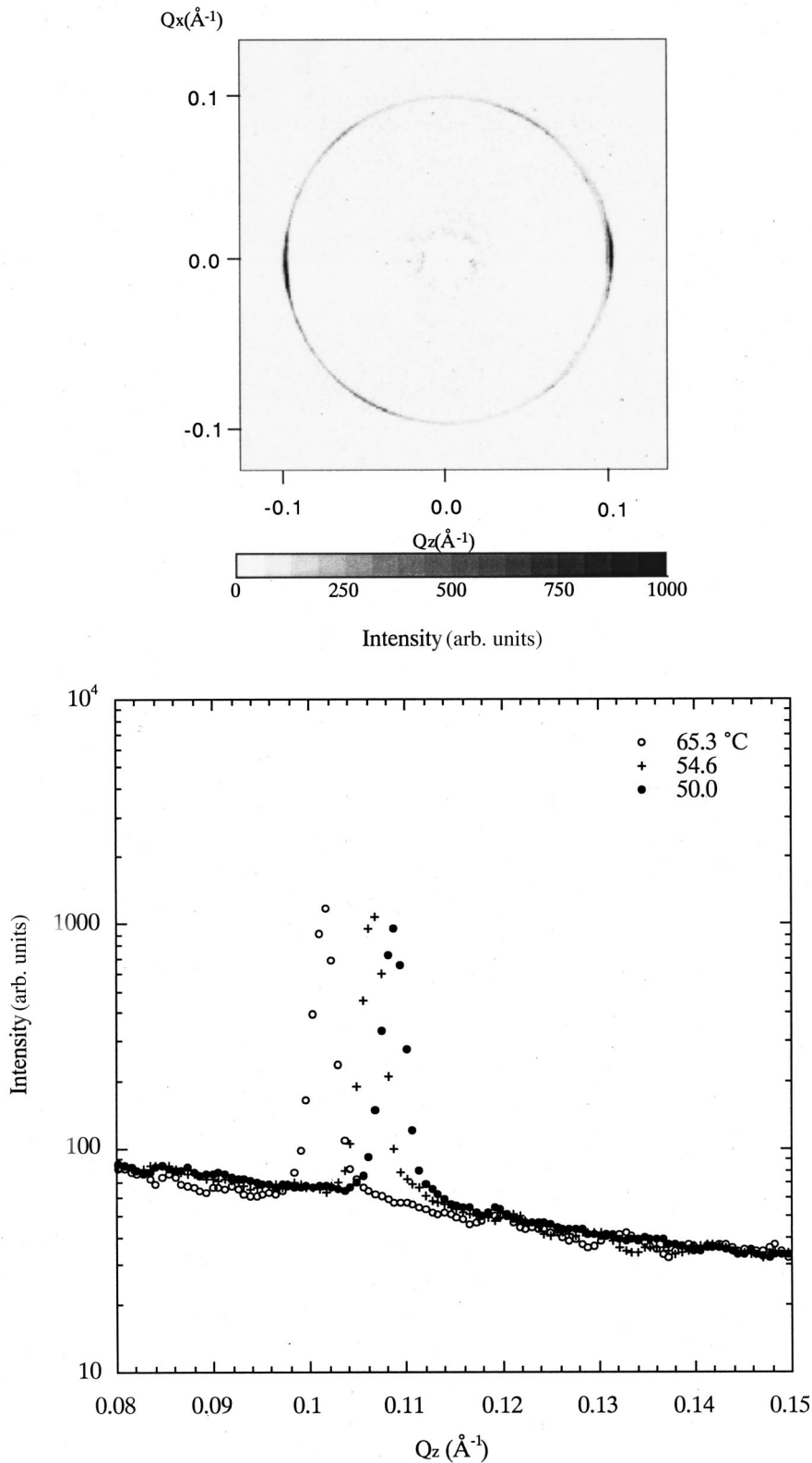


FIG. 9. (a) 2D scattering pattern $S_{\parallel}(Q_z, Q_x)$ at 63.0 °C. (b) Evolution of $S_{\parallel}(Q_z)$ from the L phase to the G phase as a function of temperature.

and lamellar periodicity $d=59.8 \text{ \AA}$ at 65 °C [30]. Thus most of the water molecules penetrate into the hydrophilic part of the surfactant bilayer. The water molecules in the hydrophilic part possibly play some roles in stabilizing the PFL structure.

Qi and Wang [27] investigated the stability of the lamellar phase using a Leibler free-energy functional. They found that anisotropic fluctuations appear when the L phase closes to its

spinodal. The dominant fluctuations will come from wave vectors on two rings at $Q_z = \pm \frac{1}{2} Q_0$ and $|Q| = Q_0$. Thus the fluctuations give a diffuse peak at $Q = \sqrt{3}/2 Q_0 = 0.87 Q_0$. Using the values of $Q_d = 0.093 \text{ \AA}^{-1}$ and $Q_0 = 0.106 \text{ \AA}^{-1}$ in our experiments at 49.5 °C (Fig. 8), we obtain the relation $Q_d = 0.88 Q_0$. Although this numerical coefficient changes in the range of 0.86–0.92 due to the temperature dependence of Q_0 , we find good agreement between the theoretical predic-

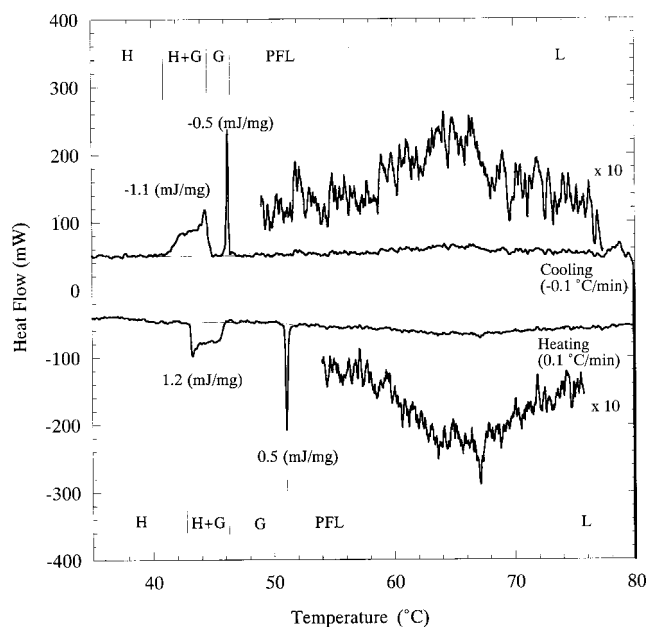


FIG. 10. DSC curves of 55 wt % $C_{16}E_7$ D_2O solution for the heating process with 0.1 $^{\circ}C/min$ and for the cooling process with 0.1 $^{\circ}C/min$.

tion and experimental results. Thus the modulation fluctuations correspond to the least stable modes of the lamellar structure near its spinodal.

According to the theory of Qi and Wang, the fluctuations diverge at the spinodal of the L phase and develop to the G phase via a body-centered-cubic-based PL structure. In Fig. 11 we show the evolution of the diffuse scattering intensity for $S_{\perp}(Q_d)$ and for the polycrystalline sample $S_{poly}(Q_d)$ as a function of temperature, $T-T_c$ where $T_c=48.3^{\circ}C(T_{LG})$. The plots of $1/S_{\perp}(Q_d)$ and $S_{poly}(Q_d)$ against $T-T_c$ give a master temperature-dependence curve. The diffuse scattering begins to grow around $T-T_c \sim 15^{\circ}C$. Decreasing the temperature to T_{LG} , the intensity increases until $T-T_c \sim 4^{\circ}C$. In the range of $T-T_c < 4^{\circ}C$, however, the growth of the diffuse scattering is suppressed and the diffuse scattering peak reaches an equilibrium profile. It is worth noting that this equilibrium temperature corresponds to the end temperature of the broad endothermic peak in the DSC profile (Fig. 9). Taking into account the fact that the peak position of the diffuse scattering in $S_{\perp}(Q)$ does not change during the cooling process, a possible explanation of the increase of $S_{\perp}(Q_d)$ with $T \rightarrow T_{LG}$ is as follows. Around $T-T_c \sim 15^{\circ}C$, amplitude-modulation fluctuations appear in lamellae. Modulation fluctuations increase their amplitude as the temperature approaches T_{LG} and finally develops to the PFL. The difference between the amplitude-modulation fluctua-

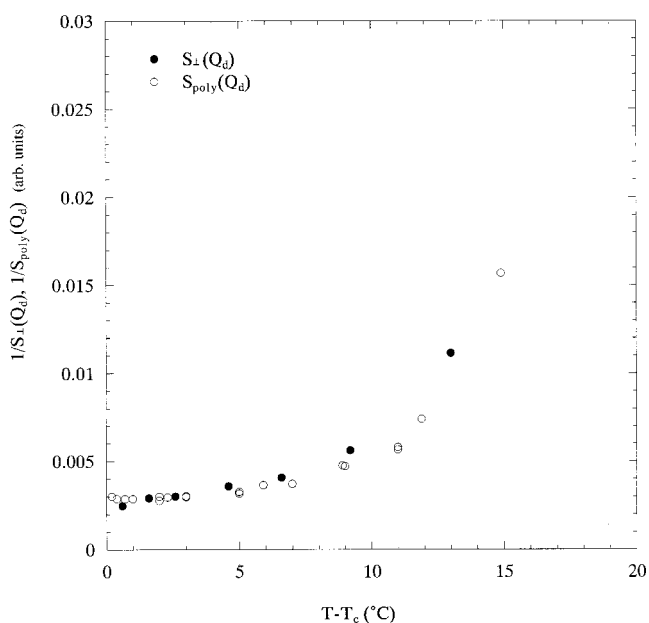


FIG. 11. Plots of $1/S_{poly}(Q_d)$ and $1/S_{\perp}(Q_d)$ against $T-T_c$, where Q_d is the position giving maximum intensity of the diffuse scattering.

tions and the perforation fluctuations is the amplitude of the fluctuations. Thus, the PFL structure may appear as a result of softening of the free-energy landscape of the lamellar phase. The PFL is an equilibrium structure in the temperature range $0 < T-T_c < 4^{\circ}C$. At the T_{LG} , first the transient R structure appears and then transforms to the G phase. It is quite interesting to note that the (110) peak of the R structure appears at the diffuse scattering peak position of the PFL structure and the (211) peak of the G phase grows at the diffuse scattering peak position of the R structure. This indicates that the fluctuations around the equilibrium ordered mesophases play an important role in the OOTs. However, the kinetic pathway from the L phase to the G phase is fairly complicated and we will discuss this matter in a future paper.

ACKNOWLEDGMENTS

We would like to express our thanks to Dr. H. Yoshida (Tokyo Metropolitan University) for DSC measurements and Mr. K. Minewaki (Tokyo Metropolitan University) for sample preparation and sample characterization. Helpful discussions with Dr. T. Ohta (Hiroshima University), Dr. T. Kawakatsu (Nagoya University), and Dr. J. Fukuda (Yokoyama Nano-Structure Liquid Crystal Project, JST) are appreciated. This work was supported by a Grant-in-Aid for Scientific Research (C) from the Ministry of Education, Science, Sports and Culture of Japan (No. 09640477).

- [1] Y. Raçon and J. Charvolin, *J. Phys. Chem.* **92**, 2646 (1988).
- [2] M. Clerc, P. Laggner, A. M. Levelut, and G. Rapp, *J. Phys. II* **5**, 901 (1995).
- [3] I. W. Hamley, K. A. Koppi, J. H. Rosedale, F. S. Bates, K. Almdal, and K. Mortensen, *Macromolecules* **26**, 5959 (1993).
- [4] D. A. Hajduk, H. Takenouchi, M. A. Hillmyer, F. S. Bates, M.

- E. Vigild, and K. Almdal, *Macromolecules* **30**, 3788 (1997).
- [5] D. A. Hajduk, R.-M. Ho, M. A. Hillmyer, F. S. Bates, and K. Almdal, *J. Phys. Chem. B* **102**, 1356 (1998).
- [6] S. Sakurai, H. Umeda, C. Furukawa, H. Irie, S. Nomura, H. H. Lee, and J. K. Kim, *J. Chem. Phys.* **108**, 4339 (1998).
- [7] M. Imai, T. Kato, and D. Schneider, *J. Chem. Phys.* **108**, 1710

- (1998).
- [8] M. Imai, K. Nakaya, and T. Kato, *Phys. Rev. E* **60**, 734 (1999).
- [9] C. Y. Ryu, M. E. Vigild, and T. P. Lodge, *Phys. Rev. Lett.* **81**, 5354 (1998).
- [10] M. Laradji, A.-C. Shi, R. C. Desai, and J. Noolandi, *Phys. Rev. Lett.* **78**, 2577 (1997).
- [11] M. Laradji, A.-C. Shi, R. C. Desai, and J. Noolandi, *Macromolecules* **30**, 3242 (1997).
- [12] S. Qi and Z.-G. Wang, *Phys. Rev. E* **55**, 1682 (1997).
- [13] M. W. Matsen, *Phys. Rev. Lett.* **80**, 201 (1998); M. Laradji, A.-C. Shi, R. C. Desai, and J. Noolandi, *ibid.* **80**, 202 (1998).
- [14] M. W. Matsen, *Phys. Rev. Lett.* **80**, 4470 (1998).
- [15] R. G. Larson, *J. Phys. II* **6**, 1441 (1996).
- [16] J. Als-Nielsen, J. D. Litster, R. J. Birgeneau, M. Kaplan, C. R. Safinya, A. Lindegaard-Andersen, and S. Mathiesen, *Phys. Rev. B* **22**, 312 (1980).
- [17] C. R. Safinya, D. Roux, G. S. Smith, S. K. Shinha, P. Dimon, N. A. Clark, and A. M. Bellocq, *Phys. Rev. Lett.* **57**, 2718 (1986).
- [18] D. Roux and C. R. Safinya, *J. Phys. (France)* **49**, 307 (1988).
- [19] A. Caillé, *C. R. Seances Acad. Sci., Ser. B* **274**, 891 (1972).
- [20] F. Nallet, R. Laversanne, and D. Roux, *J. Phys. II* **3**, 487 (1993).
- [21] Y. Amemiya, K. Wakabayashi, T. Hamanaka, T. Wakabayashi, T. Matsusita, and H. Hashizume, *Nucl. Instrum. Methods Phys. Res.* **208**, 471 (1983).
- [22] Y. Amemiya, K. Ito, N. Yagi, Y. Asano, K. Wakabayashi, T. Ueki, and T. Endo, *Rev. Sci. Instrum.* **66**, 2290 (1995).
- [23] T. Kato, N. Taguchi, T. Terao, and T. Seimiya, *Langmuir* **11**, 4661 (1995).
- [24] H. Yoshida, R. Kinoshita, and Y. Teramoto, *Thermochim. Acta* **264**, 173 (1995).
- [25] D. A. Hajduk, P. E. Harper, S. M. Gruner, C. C. Honeker, E. L. Thomas, and L. J. Fetters, *Macromolecules* **28**, 2570 (1995).
- [26] J. Burgoyne, M. C. Holmes, and G. T. T. Tiddy, *J. Phys. Chem.* **99**, 6054 (1995); C. E. Fairhurst, M. C. Holmes, and M. S. Leaver, *Langmuir* **13**, 4964 (1997).
- [27] S. Qi and Z.-G. Wang, *Macromolecules* **30**, 4491 (1997).
- [28] A. Saeki and F. Yonezawa, *Prog. Theor. Phys. Suppl.* (to be published).
- [29] T. Teramoto, A. Saeki, and F. Yonezawa, *J. Phys. Soc. Jpn.* **69**, 679 (2000).
- [30] K. Minewaki and T. Kato (unpublished).